

A new sample of large angular size radio galaxies

I. The radio data

L. Lara¹, W.D. Cotton², L. Feretti³, G. Giovannini^{3,4}, J.M. Marcaide⁵, I. Márquez¹, and T. Venturi³

¹ Instituto de Astrofísica de Andalucía (CSIC), Apdo. 3004, 18080 Granada, Spain

² National Radio Astronomy Observatory, 520 Edgemont Road, Charlottesville, VA 22903-2475, USA

³ Istituto di Radioastronomia (CNR), via P. Gobetti 101, 40129 Bologna, Italy

⁴ Dipartimento di Fisica, Università di Bologna, via B. Pichat 6/2, 40127 Bologna, Italy

⁵ Departamento de Astronomía, Universitat de València, 46100 Burjassot, Spain

Received / Accepted

Abstract. We present a new sample of 84 large angular size radio galaxies selected from the NRAO VLA Sky Survey. Radio sources with declination above $+60^\circ$, total flux density greater than 100 mJy at 1.4 GHz and angular size larger than $4'$ have been selected and observed with the VLA at 1.4 and 4.9 GHz. The radio observations attempt to confirm the large angular size sources and to isolate the core emission for optical identification. In this paper, the first of a series of three, we present radio maps of 79 sources from the sample and discuss the effects of the selection criteria in the final sample. 37 radio galaxies belong to the class of giants, of which 22 are reported in this paper for the first time.

Key words. Galaxies: active – Galaxies: nuclei – Galaxies: jets – Radio continuum: galaxies

1. Introduction

The NRAO^a VLA^b Sky Survey (NVSS; Condon et al. 1998) provides radio maps of the sky north of -40° declination, at a frequency of 1.4 GHz, in total and polarized intensity, with an angular resolution of $45''$ and 1 r.m.s. = 0.45 mJy/beam. Due to its high sensitivity and resolution compared with other all-sky surveys, the NVSS is a unique tool for the definition of complete samples of extended objects, not known before because of their low flux density and/or because of confusion effects present in previous surveys.

In 1995 we undertook a project for the definition and study of a sample of large angular size radio galaxies selected from the NVSS with the following aims:

i) To construct a sample of radio galaxies with their jets oriented near the plane of the sky and study the parsec scale properties of these jets. Most samples selected for Very Long Baseline Interferometry (VLBI) observations are usually defined on the basis of a flux density cutoff at high frequencies (eg. Pearson & Readhead 1988, Polatidis et al. 1995, Taylor et al. 1994, Kellermann et al. 1998, Fomalont et al. 2000), although it is known that the combined effect of such cutoff and the Doppler boosting

of the radio emission introduces a bias in those samples towards small orientation angles with respect to the observer's line of sight. As a consequence, only a few sources with symmetric structure on the parsec scale are currently known, despite the importance of these sources to understand the physical properties of parsec scale jets. For the selection of our sample we did not impose any core flux density limitation, and considered that simply due to projection effects, a significant number of large angular size radio sources would be oriented close to the plane of the sky and should show symmetric parsec scale jets.

ii) To study the properties of giant radio galaxies (GRGs; defined as those with a projected linear size ≥ 1 Mpc^c). This kind of source is difficult to detect: in Fanaroff-Riley type II (FR II; Fanaroff & Riley 1974) giant sources, the association between the two hotspots is often not obvious to establish; on the other hand, the low brightness extended lobes in Fanaroff-Riley type I (FR I) sources can only be detected with deep radio observations and therefore, such sources are missed in most radio surveys. Ishwara-Chandra & Saikia (1999) collected a sample of 53 GRGs from inhomogeneous literature data, but only recently, the NVSS and the Westerbork Northern Sky Survey at 325 MHz (WENSS; Rengelink et al. 1997) pro-

Send offprint requests to: L. Lara, e-mail: lucas@iaa.csic.es

^a National Radio Astronomy Observatory

^b Very Large Array, operated by the NRAO

^c We assume that $H_0 = 50 \text{ km s}^{-1} \text{ Mpc}^{-1}$ and $q_0=0.5$ throughout this paper.

vide the sufficient sensitivity to detect GRGs in a systematic way. Schoenmakers (1999) presented a sample of 47 GRGs from the WENSS survey. A new sample of large angular size radio galaxies will contain an appreciable number of intrinsically large radio galaxies and will allow us to increment the number of known GRGs. A large sample with homogeneous selection criteria is necessary to study the poorly known properties of GRGs, and how their jets interact with the external medium at large distances from the parent galaxy (Ishwara-Chandra & Saikia 1999; Schoenmakers et al. 2000; Lara et al. 2000).

iii) To investigate the evolution of radio galaxies. The selection of a sample of large angular size radio galaxies and the comparison with other samples will give new information on the time evolution of radio sources, since a larger source size implies, in principle, a higher probability of selecting older sources than in other samples (Ishwara-Chandra & Saikia 1999; Schoenmakers et al. 2000).

We present here (paper I) the sample definition and members, VLA radio maps of 79 selected objects and the main physical parameters of the sources, and we discuss the effects of the selection criteria on the sample. Papers II and III (in preparation) will present optical data (images and spectroscopy) of the associated galaxies and an analysis of the sample properties with statistical considerations, respectively.

2. Sample pre-selection

We considered all the NVSS maps above $+60^\circ$ of declination (covering an area of π steradians) and proceeded to a careful visual inspection of the contour map plots (at a 2σ level). Each $4^\circ \times 4^\circ$ NVSS map was divided in 16 $1^\circ \times 1^\circ$ maps to facilitate the search for candidates. We then pre-selected those map features apparently related to a single source, with a total flux density ≥ 100 mJy and an angular extension larger than $4'$.

Flux density measurements on the NVSS maps were done using the task TVSTAT in AIPS^d, defining a polygonal area embracing all the source emission. For the computation of the angular extension we considered the maximum distance between contours at 3σ level when the source was extended and diffuse with no evident substructure, or the distance between peaks of brightness when there were unresolved features (hotspots) at the source extremes. We took into account, when possible, curvatures in the radio structure of the sources so that a measured angular size corresponds to the length along the “spine” of the radio source. A total of 122 sources were pre-selected for subsequent confirmation through higher resolution radio observations.

We note that due to the existence of “holes” in the NVSS maps at the time of our search of candidates, a few sources fulfilling the requirements of the sample may have been skipped in the selection process and missed from

the final sample. In fact, the known giant radio galaxies 4C+73.08 (J0949+732) and 4C+74.26 (J2042+751) were not selected for the pre-sample at this first stage, but were added later to the final sample. We note however that possible missing sources will not affect the statistical considerations derived from the sample.

3. Observations and final sample selection

All the 122 pre-selected sources were observed with the VLA between 1995 and 1998 (see Table 1 for details). At least one snapshot at 1.4 and 4.9 GHz was obtained for each source. When possible, we obtained for the same source snapshots in B- and C-configurations at both frequencies to increase the image quality by combining the two different configuration data. The radio sources 3C 286 and/or 3C 48 served as primary flux density calibrators. The interferometric phases were calibrated using nearby radio sources selected from the VLA calibrator manual (Perley & Taylor 2000). The processes of self-calibration and imaging of the data were carried out with the NRAO AIPS package, following standard procedures. Due to the large size of the sources, all the maps made at 4.9 GHz and, when necessary, also at 1.4 GHz, were corrected for primary beam attenuation.

The aims of the observations were to confirm large angular size radio galaxies, reject those objects which were in fact the result of the superposition of two or three adjacent sources (see Fig. 1) and isolate the core emission to obtain accurate positions for subsequent optical identification and redshift determination.

82 of the 122 pre-selected radio sources were identified beyond doubt with single radio galaxies. 13 of those 82 sources turned out to have a size slightly smaller than $4'$ after accurate measurements from higher resolution observations. Another source has a total flux density at 1.4 GHz below 100 mJy after the subtraction of the flux density from a closely unrelated source. However, we have kept them all in the final sample since this fact will not influence our considerations. Although the integration time (10 minutes on the average) was not too long on each single source, thanks to the use of combined arrays and to the good uv-coverage of the VLA observing with the snapshot technique, we obtained the high quality images shown in Fig. 2. We present only total intensity data.

In Table 2 we report the most relevant physical parameters of the 84 radio galaxies in the final sample (82 selected objects plus the two forementioned giants 4C+73.08 and 4C+74.26). Coordinates are derived from Gaussian fits of the core component at our highest angular resolution observations (commonly 4.9 GHz, B-configuration). Total flux densities at 1.4 GHz ($S_t^{1.4}$) are from the NVSS, except when a higher resolution image is necessary to isolate and subtract discrete unrelated sources. Angular sizes are measured along the spine of the sources using our VLA maps at 1.4 GHz, or the NVSS maps when there is extended emission resolved out in our observations. The core flux density at 1.4 GHz ($S_c^{1.4}$) and 4.9 GHz ($S_c^{4.9}$) has been

^d Astronomical Image Processing System, developed and maintained by the NRAO

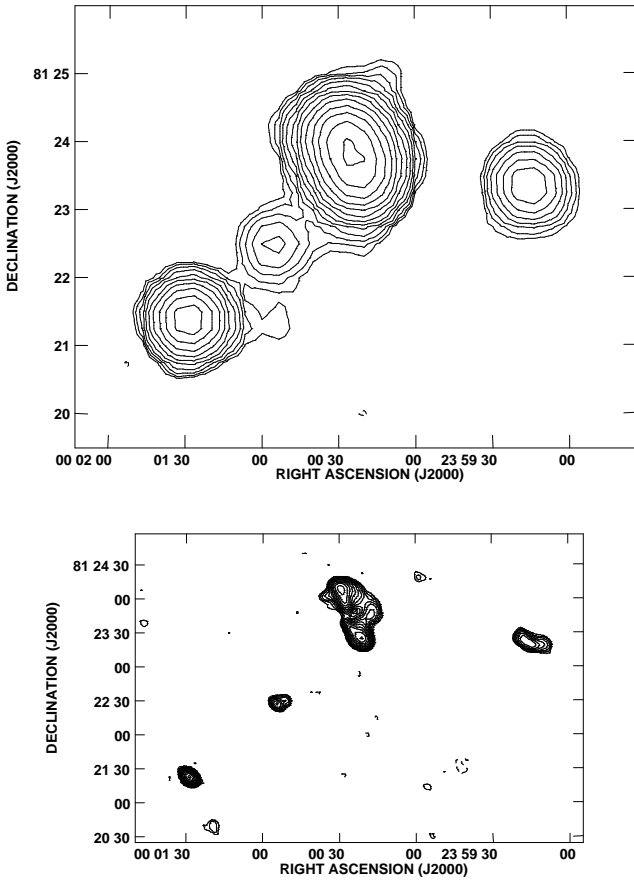


Fig. 1. Illustration of the necessity of high resolution observations of NVSS sources in order to discard some objects resulting from superposition of several unrelated sources. **Top:** an image of a presumed large size double radio galaxy selected from the NVSS. **Bottom:** the corresponding image obtained from VLA B-configuration observations at 1.4 GHz.

estimated fitting a Gaussian component to the core using AIPS task JMFIT. The peak flux density of the Gaussian was taken as the core flux density. The core peak flux densities of those sources whose cores have very different peak and integrated fluxes (peak to integrated ratio < 0.8) have been marked with an “e” in Table 2. Known redshifts have been compiled from the NASA Extragalactic Database (NED) and from Schoenmakers (1999). 44 new redshifts have been derived from our optical observations (Paper II). At present, the distance information is available for 71 of the sources (6 of which have uncertain redshift determination). When a redshift measure is available, we give also physical results as the projected linear size, the total radio power at 1.4 GHz ($P_t^{1.4}$) and the core radio power at 1.4 GHz ($P_c^{1.4}$) and 4.9 GHz ($P_c^{4.9}$).

4. Notes on individual sources

Selected radio maps of 79 objects in our sample are displayed in Fig. 2. We do not present maps of the radio sources J0318+684, J0825+693 and J1835+620, which have been discussed in separate papers (Schoenmakers et

Table 1. VLA observations

Array	ν (MHz)	$\Delta\nu$ (MHz)	Date	Code ^a
B	1465	50	19 Nov 95	<i>a</i>
C	1465	50	19 Feb 96	<i>b</i>
C	4885	100	19 Feb 96	<i>c</i>
B	1418	50	18-21 Feb 97	<i>d</i>
B	4885	100	18-21 Feb 97	<i>e</i>
B	1452	50	25 May 97	<i>f</i>
B	4885	100	25 May 97	<i>g</i>
C	1465	50	27 Jul 97	<i>h</i>
C	4885	100	27 Jul 97	<i>i</i>
B	1465	50	7 Oct 98	<i>j</i>
B	4885	100	7 Oct 98	<i>k</i>
C	1465	50	28 Dec 98	<i>l</i>
C	4885	100	28 Dec 98	<i>m</i>

^a Letter code used in Tab. 3 to show the observations made on each source.

al. 1998, Lara et al. 2000, Lara et al. 1999, respectively). We neither present maps of the sources which we have not observed: the giant radio galaxy J0949+732 (4C+73.08; Jägers 1986; Mack 1996; Leahy et al. 1998) and the giant radio quasar J2042+751 (4C74.26; Riley et al. 1989). For a few sources, images at 4.9 GHz which do not add relevant information about the source structure are not shown for brevity. The observations of each source of the sample and the parameters of each map in Fig. 2 (size and position angle (P.A.) of the convolution beam and the brightness level of the first contour) are displayed in Table 3. Unless differently commented, all the radio structure observed in the NVSS maps is also found in the presented images at 1.4 GHz. To ease the comparison of the different radio sources, we have tried to always use the same map scale at 1.4 GHz, except for those sources whose size is too large to properly fit in a single page, for which the scale has been doubled or tripled (marked with a “1/2” or “1/3” on the corresponding map). At 4.9 GHz the map scale has been optimized to show the details of the radio structure.

In the following, we briefly describe those radio sources in the sample which have peculiar properties and/or morphologies somehow different from the typical FR I or II double structure.

J0109+731 (3C 31.1): an FR II type Broad Line Radio Galaxy (BLRG) (eg. van Breugel & Jägers 1982). The NE lobe is much shorter than the SW one and in addition it has a prominent hotspot at its extreme, which suggests that the interaction with the external medium plays an important role in the source asymmetry. A jet in the SW direction is observed at 1.4 and at 4.9 GHz.

J0153+712: a low power but core dominated radio galaxy, classified as a BL-Lac candidate by Marcha et al. (1996). It is strongly asymmetric, with a wide jet directed in W-NW direction, with kinks and bends, which fades to the noise level at about $5'$ from the core in our 1.4 GHz map. We also detect a component in the opposite direction, most probably from a counter-jet. At 4.9 GHz we only detect the strong core component.

Fig.2 is provided separately as 28 .gif files

Fig. 2. VLA maps of 79 radio galaxies from the sample. A label “L” or “C” by the source name indicates the frequency of observation, namely 1.4 or 4.9 GHz, respectively. Dotted lines help to identify equivalent regions in different frequency maps. The core position is marked with an arrow on each map. The angular scale of the 1.4 GHz maps has been kept fixed, except for objects too extended to properly fit in a single page. In those cases, the map size is reduced by a factor of 2 or 3 (marked with “1/2” or “1/3” respectively). More details are provided in Table 2. Core position is marked with an arrow. Core position is marked with an arrow. Core position is marked with an arrow.

Table 2. Radio sample of large angular size radio galaxies from the NVSS survey

Name	R.A. (J2000.0) (^h ^m ^s)	Dec. (J2000.0) ([°] ['] ^{''})	S _t ^{1.4} (mJy)	Size (['])	S _c ^{1.4} (mJy)	S _c ^{4.9} (mJy)	z	Size (Kpc)	P _t ^{1.4} W/Hz	P _c ^{1.4} W/Hz	P _c ^{4.9} W/Hz	Type*
J0109+731	01 09 44.265	73 11 57.17	3030	4.0	22.0	10.0	0.181 ^a	943	26.67	24.53	24.18	II
J0153+712	01 53 25.786	71 15 06.53	1200	7.0	512.3	292.2	0.022 ^a	259	24.40	24.03	23.79	I
J0317+769	03 17 54.061	76 58 37.82	196	3.4	25.3e	11.9	0.094	476	24.89	24.00	23.67	I
J0318+684	03 18 19.026	68 29 32.08	823	15.1	22.0	44.0	0.090 ^b	2040	25.48	23.90	24.20	II
J0342+636	03 42 10.148	63 39 33.73	284	4.1	10.4	11.3	0.128	741	25.33	23.89	23.93	II
J0430+773	04 30 49.490	77 22 58.44	150	4.9	3.3	5.6	0.215	1306	25.52	23.86	24.09	II
J0455+603	04 55 47.039	60 23 36.17	109	4.0	21.5	7.3	—	—	—	—	—	I
J0502+670	05 02 54.732	67 02 30.15	104	4.8	6.9	2.3	0.085	617	24.53	23.35	22.87	I
J0508+609	05 08 27.258	60 56 27.48	221	10.4	71.0	74.8	0.071	1142	24.69	24.20	24.22	I
J0519+702	05 19 17.132	70 13 48.68	254	4.8	18.9e	11.3	0.144	952	25.38	24.26	24.03	I
J0525+718	05 25 27.094	71 52 39.25	69	4.6	4.7e	1.5	0.150	942	24.85	23.68	23.19	I
J0531+677	05 31 25.925	67 43 50.23	210	9.6	106.6e	10.6e	0.017	276	23.42	23.13	22.12	I
J0546+633	05 46 24.622	63 21 32.50	392	11.0	29.0	13.5	0.049 ^a	865	24.62	23.49	23.15	I
J0559+607	05 59 38.690	60 44 00.96	115	7.1	2.5	2.2	0.042	484	23.95	22.29	22.23	I
J0607+612	06 07 34.919	61 14 43.52	358	5.3	4.5	4.1	0.227	1465	25.94	24.04	24.00	?
J0624+630	06 24 29.063	63 04 02.50	181	5.4	3.5	4.4	0.085	694	24.77	23.05	23.15	I
J0633+721	06 33 40.842	72 09 24.92	308	5.0	14.0	12.0	0.090 ^b	675	25.05	23.71	23.64	?
J0654+733	06 54 26.525	73 19 50.36	868	12.2	3.2	4.1	0.115 ^b	2015	25.71	23.28	23.39	II
J0750+656	07 50 34.425	65 41 25.50	120	3.7	26.8	29.4	0.747	1798	26.57	25.92	25.96	II
J0757+826	07 57 35.172	82 39 40.86	153	4.0	33.7	17.1e	0.087 ^c	524	24.71	24.06	23.76	I
J0803+669	08 03 45.829	66 56 11.39	182	4.7	5.2	3.8	0.247 ^c	1374	25.73	24.18	24.04	II
J0807+740	08 07 10.070	74 00 41.58	152	9.1	14.0	12.4	0.120 ^b	1566	25.00	23.96	23.91	?
J0819+756	08 19 50.504	75 38 39.53	616	7.8	30.7	56.6	0.232 ^b	2190	26.20	24.90	25.16	II
J0825+693	08 25 59.770	69 20 38.59	141	7.2	7.1	7.1	0.538 ^a	3162	26.33	25.03	25.03	II
J0828+632	08 28 56.363	63 13 45.05	182	4.0	6.3	3.7	—	—	—	—	—	?
J0856+663	08 56 16.260	66 21 26.50	236	3.8	5.3	10.3	0.489	1607	26.47	24.82	25.11	II
J0926+653	09 26 00.822	65 19 22.88	101	5.3	1.0e	2.2e	0.140	1028	24.96	22.95	23.30	I
J0926+610	09 26 53.408	61 00 24.87	300	3.7	6.8	7.2	0.243	1070	25.93	24.28	24.31	II
J0939+740	09 39 46.833	74 05 30.78	100	8.0	3.9	4.5	0.122 ^b	1387	24.83	23.42	23.48	I
J0949+732 ^c	09 49 46.157	73 14 23.82	2537	15.0	15.6	20.0	0.058 ^a	1375	25.58	23.37	23.47	II
J1015+683	10 15 21.620	68 23 58.24	390	4.0	—	5.6	0.199	1010	25.86	—	24.02	?
J1036+677	10 36 41.237	67 47 53.44	231	4.0	2.6	3.8	—	—	—	—	—	II
J1124+749	11 24 47.045	74 55 45.31	125	5.6	38.4	23.8	0.052	465	24.17	23.66	23.45	I
J1137+613	11 37 21.289	61 20 01.88	1160	3.4	13.1e	12.5	0.111	549	25.81	23.87	23.85	II
J1211+743	12 11 58.710	74 19 04.12	628	7.5	9.7	11.3	0.107	1171	25.51	23.70	23.77	?
J1216+674	12 16 37.239	67 24 41.97	187	5.8	2.0	3.2	0.362	2126	26.09	24.12	24.32	II
J1220+636	12 20 36.477	63 41 43.82	261	5.2	4.2	6.4	—	—	—	—	—	II
J1247+673	12 47 33.319	67 23 16.34	388	12.4	262.4	179.0	0.107 ^a	1938	25.30	25.13	24.97	II
J1251+756	12 51 05.977	75 37 38.94	100	4.0	2.9	4.4	0.197	1002	25.26	23.72	23.90	II
J1251+787	12 51 23.839	78 42 36.29	166	19.5	13.2	15.5	—	—	—	—	—	I
J1313+696	13 13 58.878	69 37 18.74	1384	6.9	10.2e	3.8	0.106 ^a	1062	25.85	23.71	23.29	II
J1410+633	14 10 30.609	63 19 00.55	249	3.4	3.1e	1.1e	0.158	724	25.46	23.55	23.10	II

* I and II stand for FR I and FR II type radio galaxies, respectively

^a Redshift taken from the NASA Extragalactic Database^b Redshift from Schoenmakers (1999)^c Coordinates taken from Saripalli et al. (1997)

Label “e” by the core flux density means extended core (see text).

New giant radio galaxies are written in boldface.

J0317+769: presents a peculiar morphology consisting of a core and two FR I type symmetric and prominent jets, which end in two FR II type lobes (better seen in the 4.9 GHz map). From the SW lobe, a faint and extended tail rises directed in S direction (1.4 GHz map). This tail is completely resolved out in our 4.9 GHz map.

J0455+603: a peculiar radio source with a well defined core embedded in a low brightness halo-like structure in NW-SE direction. Our 1.4 GHz map shows marginal evidence of a jet in NW direction. No redshift information is available for this radio source.

J0508+609: a low power FR I type giant radio galaxy with a prominent flat spectrum core and two opposite jets directed in SE-NW direction. Both jets present large opening angles. The northern jet can be followed at larger distances from the core than the southern one, which is resolved out beyond 1.25' from the core in our map at 1.4 GHz, but clearly seen in the NVSS map up to 6' from the core. At 4.9 GHz we only detect the core component,

a 13'' jet in SE direction and marginal evidence of the counter-jet on the opposite side.

J0525+718: a low power radio galaxy with two symmetric jets in the E-W direction. The western jet shows a 90° bend in projection towards the north. It is not clear if this bend is somehow related to a compact source seen in the same field. The total flux density of J0525+718 at 1.4 GHz is below the 100 mJy limit after the subtraction of the flux density from this compact source, but we have kept it in the final sample. At 4.9 GHz we only detect a weak core component and a very faint jet and counter-jet emission (map not shown).

J0531+677: our 4.9 GHz map shows a weak core and two symmetric jets in the NE-SW direction, typical of an FR I structure. What is peculiar in this radio source is the existence of a very faint and extended tail directed towards the south, similar to that previously described in J0317+769. A similar tail might be present in the other jet as in wide angle tail radio galaxies, but the emission

Table 2. (*cont.*) Radio sample of large angular size radio galaxies from the NVSS survey

Name	R.A. (J2000.0) (^h ^m ^s)	Dec. (J2000.0) (^o ['] ^{''})	S _c ^{1.4} (mJy)	Size (['])	S _c ^{1.4} (mJy)	S _c ^{4.9} (mJy)	z	Size (Kpc)	P _t ^{1.4} W/Hz	P _c ^{1.4} W/Hz	P _c ^{4.9} W/Hz	Type*
J1504+689	15 04 12.781	68 56 12.75	451	3.4	88.4	72.1	0.318 ^a	1160	26.35	25.64	25.55	II-QSS
J1523+636	15 23 45.900	63 39 23.78	676	3.5	18.3e	14.5	0.204 ^a	899	26.12	24.55	24.45	II
J1530+824	15 30 56.110	82 27 21.02	180	6.6	40.6	27.2e	0.021 ^a	236	23.55	22.90	22.73	I
J1536+843	15 36 57.335	84 23 10.42	375	8.0	4.9	3.3	0.201 ^b	2033	25.85	23.97	23.80	II
J1557+706	15 57 30.190	70 41 20.79	1800	11.3	25.2	31.3	0.026 ^a	490	24.72	22.87	22.96	I
J1632+825	16 32 31.630	82 32 16.28	2200	66.0	428.2	286.0	0.023 ^a	2544	24.70	23.99	23.82	I
J1650+815	16 50 58.686	81 34 28.11	313	5.6	44.4	32.8	0.038 ^a	348	24.30	23.45	23.32	I
J1732+714	17 32 33.001	71 24 10.50	616	4.0	35.1e	9.5e	0.059 ^a	372	24.98	23.73	23.16	I
J1733+707	17 33 12.525	70 46 30.36	240	4.5	10.6e	8.1	0.041 ^a	299	24.24	22.89	22.77	I
J1743+712	17 43 17.681	71 12 53.98	142	4.0	9.2	13.1	—	—	—	—	—	II
J1745+712	17 45 43.573	71 15 48.55	883	4.4	25.9e	10.9	0.216 ^a	1176	26.29	24.76	24.38	II
J1751+680	17 51 19.629	68 04 43.05	153	8.1	11.8e	9.0	0.079	978	24.63	23.52	23.40	I
J1754+626	17 54 50.310	62 38 41.96	991	16.2	5.0	5.6	0.028 ^a	754	24.53	22.23	22.28	I
J1800+717	18 00 42.622	71 44 41.99	144	4.2	1.4	0.9	—	—	—	—	—	II
J1835+665	18 35 07.338	66 35 00.02	136	4.4	2.9	1.6	0.354 [?]	1594	25.93	24.26	24.00	II
J1835+620	18 35 10.405	62 04 07.42	800	3.9	2.0e	1.7	0.518	1688	27.05	24.45	24.38	II
J1844+653	18 44 07.443	65 22 03.07	104	7.5	0.8	1.9	0.197	1881	25.28	23.16	23.54	II
J1845+818	18 45 15.836	81 49 30.98	596	4.4	5.2	6.9	0.119	750	25.58	23.52	23.65	II
J1847+707	18 47 34.912	70 44 00.64	226	3.8	31.2e	8.1e	0.043	265	24.26	23.40	22.82	I
J1850+645	18 50 45.871	64 30 24.68	154	5.6	10.6e	4.0e	0.080	683	24.64	23.48	23.06	I
J1853+800	18 53 52.077	80 02 50.46	155	5.6	3.4e	2.1	0.214 ^a	1486	25.53	23.87	23.66	II
J1918+742	19 18 34.885	74 15 05.05	570	6.6	26.1	8.8	0.194	1636	26.00	24.66	24.19	II
J1951+706	19 51 40.825	70 37 39.99	100	5.2	3.4	6.0	0.550	2303	26.20	24.74	24.98	II
J2016+608	20 16 18.630	60 53 57.49	332	3.0	2.3e	2.2	0.121	519	25.35	23.19	23.17	II
J2035+680	20 35 16.549	68 05 41.60	156	11.5	10.6	15.5	0.133	2143	25.10	23.93	24.10	I
J2042+751 ^c	20 42 37.180	75 08 02.52	1805	10.6	184.0	328.0	0.104 ^a	1617	25.94	24.95	25.20	II-QSS
J2059+627	20 59 09.560	62 47 44.11	113	4.7	3.0	4.0	0.267	1444	25.59	24.01	24.14	II [?]
J2103+649	21 03 13.868	64 56 55.26	123	4.8	9.8	7.3e	0.215	1279	25.43	24.33	24.20	II
J2111+630	21 11 20.268	63 00 06.17	285	7.0	—	1.0	—	—	—	—	—	II
J2114+820	21 14 01.179	82 04 48.28	483	6.0	141.1	140.9	0.085	772	25.19	24.66	24.66	I
J2128+603	21 28 02.634	60 21 07.96	258	5.9	4.5e	6.4	0.072 [?]	656	24.77	23.02	23.17	II
J2138+831	21 38 42.266	83 06 49.21	305	5.1	30.2	13.8	0.135	962	25.41	24.40	24.06	?
J2145+819	21 45 29.887	81 54 54.22	400	18.7	12.0	8.2	0.146 ^b	3739	25.59	24.07	23.90	II
J2157+664	21 57 02.572	66 26 10.24	1070	5.0	—	34.6	0.057 [?]	451	25.19	—	23.70	?
J2204+783	22 04 09.225	78 22 46.92	251	4.0	3.4	5.4	0.115	663	25.18	23.31	23.51	II
J2209+727	22 09 33.780	72 45 58.36	248	3.7	—	0.4	0.201	940	25.67	—	22.88	II
J2242+622	22 42 32.133	62 12 17.53	287	4.2	1.6	1.9	0.188 [?]	1018	25.68	23.42	23.50	II
J2247+633	22 47 29.714	63 21 15.55	477	4.4	6.7e	4.2	—	—	—	—	—	I
J2250+729	22 50 43.621	72 56 16.19	653	3.8	—	0.9e	—	—	—	—	—	II
J2255+645	22 55 29.943	64 30 06.86	392	4.0	4.9	7.3	—	—	—	—	—	II
J2307+640	23 07 58.533	64 01 39.22	171	4.6	7.3	4.3	—	—	—	—	—	II
J2340+621	23 40 56.435	62 10 45.09	185	4.1	2.0	2.6	—	—	—	—	—	I

* I and II stand for FR I and FR II type radio galaxies, respectively

^a Redshift from the NASA Extragalactic Database^b Redshift from Schoenmakers (1999)^c Core flux densities taken from Pearson et al. (2000).

Label “e” by the core flux density means extended core (see text).

New giant radio galaxies are written in boldface.

quickly fades below the noise level. It is the nearest object in the sample, at $z=0.017$.

J0546+633: an asymmetric FR I type radio galaxy with a NE-SW orientation. The jet and counter-jet are prominent in our maps and well collimated. While the SW jet fades away as it separates from the core, the NE jet is shorter and presents a strong bending backwards. This is another example of a radio galaxy with an asymmetric structure, possibly resulting from different degrees of interaction of the oppositely directed jets with the external medium and/or the projection effects.

J0607+612: a radio galaxy with lobes in the NE-SW direction. Its projected linear size is 1.47 Mpc (GRG). At 4.9 GHz we can clearly follow the jet directed towards the NE lobe. The structure of J0607+612 cannot be easily classified as an FR I or FR II type.

J0624+630: a low power FR I radio source oriented in N-S direction with an S-shaped morphology. The N-jet presents a strong bend at 0.7' from the core. The core component is clearly identified in the 4.9 GHz map.

J0654+733: a 2 Mpc long FR II radio galaxy directed in the NE-SW direction, with prominent hotspots at the lobe extremes. The core is displaced towards the SW with respect to the center of symmetry of the source. A background compact source, most probably unrelated, is located close to the northern lobe.

0750+656: the most distant object of our sample, at $z=0.747$. It is a GRG with a linear projected size of 1.8 Mpc. It presents a prominent core and a FR II type radio structure in NW-SE direction.

J0807+740: a giant low power radio galaxy. At 1.4 GHz, this peculiar radio source presents a compact core component and a weak and extended halo-like emission elongated in the E-W direction. There is no evidence of jets or hotspots in our maps. At 4.9 GHz we only detect the core component. This object could be a relic FR II radio galaxy, where hotspot regions are no more present and extended lobes are still detected at 1.4 GHz.

J0819+756: an FR II type GRG (linear size of 2.2 Mpc) oriented in NE-SW direction. It presents a strong

Table 3. Map parameters

Name	Observations ^a	1.4 GHz			4.9 GHz		
		Beam "×"	P.A.	1st contour mJy/beam	Beam "×"	P.A.	1st contour mJy/beam
J0109+731	j,k	5.9×3.7	-39.6	0.86	1.7×1.7	–	0.39
J0153+712	j,k,l	10.7×9.6	-31.9	1.0	–	–	N.S.
J0317+769	b,c,d,g,l	22.0×12.1	-68.0	0.7	3.7×2.9	-88.3	0.15
J0318+684	a,b,c	–	–	N.S. ^b	–	–	N.S.
J0342+636	b,f,k	10.6×9.7	68.8	0.45	1.5×1.5	–	0.16
J0430+773	b,c,f,g	10.6×10.2	82.9	0.6	3.8×3.0	-68.9	0.18
J0455+603	b,c,f	5.9×4.7	46.1	0.14	–	–	N.S.
J0502+670	b,c,f,k	10.7×9.9	89.2	0.2	3.3×3.1	-64.6	0.1
J0508+609	a,b,c,g	15.0×10.2	-74.5	0.2	3.3×2.8	63.0	0.2
J0519+702	a,b,c,g	13.4×10.4	82.4	0.4	4.4×2.8	-56.1	0.1
J0525+718	a,b,c,g	13.3×10.0	83.1	0.4	–	–	N.S.
J0531+677	b,c,d,g	25.0×25.0	–	0.8	1.6×1.6	–	0.17
J0546+633	a,b,c,g	15.4×10.5	-67.8	0.25	4.2×3.1	72.6	0.1
J0559+607	b,c,f	11.2×9.3	59.5	0.2	–	–	N.S.
J0607+612	a,b,c,k	15.2×11.5	-68.8	0.4	4.1×3.0	59.0	0.1
J0624+630	b,c,f,g	11.2×9.5	66.0	0.3	3.9×3.3	69.3	0.1
J0633+721	a,b,c,g	13.2×10.9	-82.3	0.3	4.6×2.7	44.0	0.1
J0654+733	a,b,c	16.2×12.5	60.6	0.4	–	–	N.S.
J0750+656	d,h,k	9.2×4.8	-80.9	0.5	1.7×1.7	–	0.15
J0757+826	d,h,m	22.0×22.0	–	5.0	6.1×6.1	–	0.3
J0803+669	b,c,f	6.7×4.7	58.9	0.35	–	–	N.S.
J0807+740	a,b,c	13.0×11.3	-30.2	0.3	–	–	N.S.
J0819+756	a,b,c,g	13.9×12.6	13.2	0.3	7.7×7.7	–	0.4
J0825+693	a,b,c,g	–	–	N.S.	–	–	N.S.
J0828+632	d,h,k	9.8×6.3	-72.1	0.4	1.7×1.7	–	0.15
J0856+663	b,c,f	13.4×13.4	–	0.6	–	–	N.S.
J0926+653	d,h,m	26.0×26.0	–	1.3	6.1×6.1	–	0.15
J0926+610	d,k	12.3×4.8	-63.8	0.7	1.7×1.7	–	0.14
J0939+740	b,c,f	12.0×12.0	–	0.6	7.0×7.0	–	0.15
J0949+732	–	–	–	N.S.	–	–	N.S.
J1015+683	d,g,h,i	12.2×4.8	-58.0	0.6	4.8×3.6	-11.7	0.13
J1036+677	d,e,h,i	12.4×4.8	-58.1	0.45	5.5×3.2	-59.7	0.1
J1124+749	f,h,m	25.0×25.0	–	0.5	6.8×6.8	–	0.15
J1137+613	d,m	9.0×9.0	–	1.0	7.3×7.3	–	0.2
J1211+743	f,g,h,i	12.0×12.0	–	0.4	4.4×3.8	-32.9	0.1
J1216+674	d,m	8.5×8.5	–	0.5	–	–	N.S.
J1220+636	d,l,m	8.9×8.9	–	0.9	7.3×7.3	–	0.16
J1247+673	d,e,l	26.0×26.0	–	1.0	–	–	N.S.
J1251+756	f,h,m	12.6×11.3	39.0	0.3	6.8×6.8	–	0.1
J1251+787	d,e,h,i	24.0×24.0	–	0.5	5.4×3.4	-29.6	0.1
J1313+696	d,e	8.0×8.0	–	0.9	2.5×2.5	–	0.5
J1410+633	d,m	10.0×10.0	–	0.6	8.4×8.4	–	0.3

^a The codes in this column refer to those in Table 1

^b N.S. stands for not shown sources in Fig. 2

inverted spectrum core ($\alpha_{1.4}^{4.9} = 0.5$; Flux density $\propto \nu^\alpha$). Both lobes harbour a double hotspot structure at their extremes. The source beyond the NE lobe is an unrelated background object, as suggested by its structure and its optical identification.

J1015+683: presents a very complex and distorted structure oriented in the E-W direction resembling, mostly at 4.9 GHz, two double radio galaxies closely seen in projection, one slightly above the other. This is supported by the optical image which shows two nearby galaxies in the field identified with radio components (Paper II). Redshift and core data on Table 2 refer to the northern feature.

J1137+613: a symmetric radio galaxy of FR II type morphology with prominent hotspots at the end of the lobes. There is evidence of a strong backflow from both radio lobes which is deflected in opposite directions perpendicularly to the axis defined by the jets.

J1211+743: a GRG (linear size of 1.2 Mpc) which presents a peculiar structure, not clearly discriminated between FR I or II types. There is a prominent jet in the NW direction, showing blobs of emission and a bent structure. A faint counter-jet is also detected. No strong hotspots are observed in the lobes.

J1247+673: a known Gigahertz Peaked Spectrum radio galaxy with a FR II type morphology (de Vries et al. 1997), also a member of the class of giant radio galaxies (linear size of 1.94 Mpc). It clearly contrasts with respect to the rest of the sample in its core dominance (67% of the source emission at 1.4 GHz comes from the core, which is the only feature detected at 4.9 GHz).

J1251+787: one of the most extended radio galaxies in our sample (19.5'; redshift is not available for this source). It presents a FR I type morphology, with two irregular S-shaped and well collimated jets. They present several blobs of emission and bends until they fall below the noise level of our images.

J1313+696 (4C+69.15): an FR II type radio galaxy oriented in SE-NW direction. With a projected linear size of 1.06 Mpc, it belongs to the class of giants. At 1.4 GHz the emission from the lobes form a continuous bridge along the entire source. At 4.9 GHz only the core and the lobe extremes are detected. This case emphasizes the importance of the observations made at 4.9 GHz to discriminate the core component, needed to identify the associated galaxy.

Table 3. (*cont.*) Map parameters

Name	Observations ^a	1.4 GHz		4.9 GHz	
		Beam "×"	P.A.	Beam "×"	P.A.
J1504+689	d,k	10.0×10.0		1.8×1.8	0.3
J1523+636	d,e	11.0×11.0	0.8	3.1×3.1	0.22
J1530+824	f,h,m	25.0×25.0	1.0	6.7×6.7	0.15
J1536+843	f,h,m	9.8×5.2	80.6	6.6×6.6	0.15
J1557+706	d,g,l	10.9×8.9	77.0	2.0×2.0	0.25
J1632+825	f,g,h,i	13.9×9.5	69.9	3.3×3.3	0.2
J1650+815	f,h,m	25.0×25.0	0.63	6.6×6.6	0.2
J1732+714	d,e	9.0×4.8	-60.6	2.8×1.4	-78.0
J1733+707	d,m	7.9×6.7	-3.1	6.6×6.6	0.14
J1743+712	d,g,l	7.4×5.0	-66.0	1.8×1.8	0.16
J1745+712	d,g,l	8.0×5.7	-78.5	1.8×1.8	0.2
J1751+680	d,k,l	6.9×4.7	-64.2	1.8×1.4	-23.2
J1754+626	d,g,l	24.0×24.0	0.8	1.8×1.8	0.15
J1800+717	d,k	7.1×4.7	-61.8	–	N.S. ^b
J1835+665	d,m	6.8×4.7	-58.4	6.8×6.8	0.2
J1835+620	d,e,l,m	–	N.S.	–	N.S.
J1844+653	d,l,m	24.0×24.0	1	7.0×7.0	0.14
J1845+818	f,h,m	13.8×9.4	87.7	6.3×6.3	0.14
J1847+707	d,e,l	12.2×10.1	-87.6	2.2×1.4	-60.1
J1850+645	d,g,l	25.0×25.0	1.0	–	N.S.
J1853+800	f,g,h,i	14.2×9.6	86.7	5.0×3.4	74.6
J1918+742	j,k,l	13.0×13.0	0.8	–	N.S.
J1951+706	j,l,m	12.5×12.5	0.35	6.8×6.8	0.2
J2016+608	j,k	6.2×4.9	-50.6	1.7×1.7	0.15
J2035+680	j,k,l	22.0×22.0	0.65	1.7×1.7	0.15
J2042+751	–	–	N.S.	–	N.S.
J2059+627	j,m	5.5×5.5	0.5	7.0×7.0	0.15
J2103+649	j,l,m	11.7×10.2	84.3	6.7×6.7	0.16
J2111+630	j,k,l	22.0×22.0	1.0	–	N.S.
J2114+820	a,b,c,g,j,k	12.8×9.7	11.1	2.9×2.3	-65.5
J2128+603	j,k	5.4×3.8	-51.5	1.7×1.7	0.15
J2138+831	a,b,c,g	12.8×9.6	16.7	6.5×3.4	40.8
J2145+819	a,b,c	12.7×9.8	19.0	–	N.S.
J2157+664	j,k,l,m	11.6×10.1	87.5	4.1×3.2	88.5
J2204+783	a,b,c,g	13.0×10.2	34.1	4.1×3.0	45.1
J2209+727	j,k	7.4×5.2	-57.7	1.8×1.8	0.22
J2242+622	j,k	5.1×3.8	-36.9	1.6×1.6	0.14
J2247+633	j,k	6.3×5.0	-45.1	1.6×1.6	0.1
J2250+729	j,k	7.2×4.9	-51.7	1.8×1.8	0.2
J2255+645	j,k	6.8×4.8	-60.2	–	N.S.
J2307+640	j,k	5.7×3.7	-53.9	–	N.S.
J2340+621	j,k	5.5×3.8	-50.1	1.6×1.6	0.15

^a The codes in this column refer to those in Table 1

^b N.S. stands for not shown sources in Fig. 2

J1504+689 (4C+69.18): one of the few quasars in the sample, presents a typical FR II type morphology with a bright flat-spectrum core and two lobes with prominent hotspots. With a projected linear size of 1.16 Mpc, it is a giant radio quasar. There is an unrelated strong compact source at 2.16' from the core, in SW direction, which was misidentified with a component of J1504+689 by Reid et al. (1995).

J1557+706 (4C+70.19): it presents an FR I type morphology in the N-S direction. The northern jet bends by 180° towards the south, becoming diffuse and extended beyond the bend. The southern jet ends in an extended lobe-like region. At 4.9 GHz we only detect a compact core and the beginning of two rather symmetric jets, separated from the core by symmetric gaps.

J1632+825 (NGC 6251): a very well studied radio galaxy (eg. Perley et al. 1984), and the most extended one in our sample (66' ≡ 2.54 Mpc). Our observations show only a prominent and well collimated one-sided jet in the NW direction, with no evidence of the counter-jet emission. Total angular size and total flux density in Table 2 are from Perley et al. (1984).

J1650+815: a peculiar low brightness asymmetric radio galaxy. The core is clearly identified at 4.9 GHz, and appears displaced towards the north with respect to the center of the radio structure. There is evidence of a jet departing from the core in S-SW direction, and two extended and diffuse lobes.

J1732+714: an FR I type radio galaxy with two symmetric jets departing from a central core. The jets end in two extended lobes without strong hotspots. It presents a bridge of low brightness emission southward of the jets and in the same direction, very much like the relic emission observed in 3C 338 (Giovannini et al. 1998).

J1745+712 (4C+71.17): at 1.4 GHz it shows an FR II type morphology in the E-W direction with a dominant bright emission from the core region. Higher resolution observations at 4.9 GHz show a small and prominent structure (~ 15'') with a core and a two symmetric jet components, which might be the result of an episode of enhanced activity, as in the case of J1835+620 (Lara et al. 1999).

J1751+680: a wide angle tail radio source with detached lobes displaced towards the east. The southern jet presents a sharp bend of ~ 90°. An unrelated double radio

source appears confused with the southern lobe when observed at low angular resolution (e.g. in the NVSS map).

J1754+626 (NGC 6512): another wide angle tail source, with an extension of low brightness emission in the southern direction. The radio structure is very complex, with sharp bends and kinks, most likely produced by the interaction with the external medium. At 4.9 GHz we observe the core component and two jets in the E-W direction. The eastern jet bends sharply towards the west, most probably due to the existence of a strong intergalactic wind.

J1918+742: a GRG with projected linear size of 1.64 Mpc. It presents an FR II type morphology in the E-W direction, with the core strongly displaced towards the east from the center of symmetry of the source. At 4.9 GHz we only detect the core and the hotspot in the western lobe.

J2035+680: an FR I type radio galaxy in the N-S direction with two extended and diffuse lobes. The northern jet presents a prominent blob of emission at $2'$ from the core. The angular size is $11.5'$, which correspond to 2.14 Mpc in projected linear size for a redshift $z=0.133$ (uncertain). There is a strong and compact radio source almost superposed to the southern lobe, which we consider unrelated to J2035+680.

J2111+630: a peculiar source with an FR II type morphology in the NW-SE direction. At 1.4 GHz, the lobes appear extended with signs of backflow, but there are not prominent hotspots. At 4.9 GHz we only detect a weak core (flux density ~ 1 mJy). We could not determine the redshift of the associated galaxy.

J2114+820: presents an FR I type structure, with S-shaped extended lobes and a strong and variable flat spectrum core (variability observed in our data at different epochs). There is a prominent jet in the NW direction with several blobs of emission and with a very strong widening at about $\sim 20''$ from the core. A weaker counter-jet is observed on the opposite side. Its optical spectrum presents prominent broad emission lines (Stickel et al. 1993; Paper II), which according with current unification schemes of radio loud Active Galactic Nuclei (e.g. Urry & Padovani 1995), is in contradiction to its classification as an FR I radio galaxy (see also Lara et al. 1999).

J2138+831: a strongly asymmetric radio galaxy in the cluster Abell 2387. While the eastern lobe bends southwards forming a long tail of FR I type, the western lobe resembles those found in FR II type radio sources. At 4.9 GHz we observe how the jet directed towards the west loses its collimation at $\sim 30''$ from the core.

J2145+819: an FR II type radio galaxy with a N-S orientation. It is the intrinsically largest radio galaxy in our sample (a giant among the giants, with a projected linear size of 3.74 Mpc). The northern lobe presents an almost perfect conical shape with a prominent hotspot at its extreme (see Lara et al. 2000). Palma et al. (2000) present a detailed study of this radio source.

J2157+664 (4C66.24): a very peculiar and asymmetric radio source. At first sight (1.4 GHz observations)

it seems to have two typical radio lobes in the E-W direction, one of them with a strong hotspot. However, observations at 4.9 GHz and spectral index considerations show that the core is hosted by the western “lobe”, and that a jet directed towards the west interacts at a very short distance from the core with the external medium, producing a very strong bow-shock. On the opposite side, there is a long jet which seems to bend in an almost closed loop, forming a long tail of low brightness emission towards the south (observed at 1.4 GHz).

J2209+727: an FR II type radio galaxy in the NW-SE direction. The core is very weak and appears confused with the lobe emission at 1.4 GHz. At 4.9 GHz we can clearly identify the weak core (flux density $400\mu\text{Jy}$) and the hotspots at the extremes of the lobes. There are two nearby radio sources in the same field, most probably unrelated with J2209+727.

J2340+621: a peculiar radio source extended in the E-W direction, with two collimated S-shaped jets. In both jets there are prominent blobs of emission at $\sim 22''$ (E-jet) and $\sim 30''$ (W-jet) from the core, which suggest different phases in the core activity, as in the case of J1745+712 or J1835+620 (Lara et al. 1999). This radio source is located at a very low galactic latitude, 0.4° . We detected its optical counterpart, although its extragalactic nature could not be confirmed (Paper II).

5. Discussion

We discuss in this section possible biases introduced in our sample due to the criteria adopted for the sample selection and to the sensitivity limitations of the NVSS. A detailed discussion about the implications on the radio source population derived from the sample is left for a forthcoming paper (Paper III).

In Fig. 3 we represent the flux density per length unit against the source angular size for all the members of the sample. In this plot we can clearly see the limitations imposed by the selection criteria. The vertical solid line represents the lower limit in angular size ($4'$). As mentioned in Section 3, there are 13 sources with sizes below that limit, which have been kept in the sample. The oblique solid line represents the lower limit in total flux density (100 mJy). There is one source (J0525+718) which lies below that limit (Section 3). The horizontal dashed line marks the limit imposed by the NVSS sensitivity ($1\sigma = 0.45$ mJy/beam), computed considering a rectangular source with a fixed width of $3'$ (an upper limit inferred from the NVSS maps), a variable length l and an uniform brightness distribution at 3σ . The intersection of this line with the flux density limit line (P point) defines the length ($l \sim 16'$) above which sources with flux densities above 100 mJy could be missed in our sample.

In order to investigate if such very extended sources could be more properly studied using a lower frequency survey, we have cross-checked our sample with a sample of 47 low redshift ($z \leq 0.4$) GRGs with angular sizes larger than $5'$ selected from the WENSS (Schoenmakers 1999).

Two radio galaxies, J1047+747 and J1308+619, appear in this sample and are not present in our sample due to their low total flux densities at 1.4 GHz, but not to their too large size. The rest of the sources in Schoenmakers sample with declination $\geq +60^\circ$ are also in our sample. On the other hand, we find 8 low redshift GRGs with angular sizes larger than $5'$ that are missing from Schoenmakers sample, most possibly due to an underestimation of the true source size induced by the low resolution of the WENSS survey (Schoenmakers priv. comm.). These 8 sources are J0607+612, J0926+653, J1216+674, J1844+653, J1853+800, J1918+742, J1951+706 and J2035+680. We have also checked that all giant radio galaxies larger than $4'$ in the compilation by Ishwara-Chandra & Saikia (1999) are in our sample. Therefore, we have enough confidence that the selection from the NVSS is a good procedure (at least as good as others) to define samples of extended radio sources. In fact, we find in our sample 22 new GRGs (written in boldface in Table 2), increasing to a total of 103 the number of known giants.

Fig. 4 shows the number of sources per redshift bin of 0.05. We find that 87% of the sources with known redshift are below $z=0.25$. In fact, the selection criteria require sources with $z \geq 0.5$ to have projected linear sizes larger than 1.7 Mpc (see Fig. 6). Since such huge sources are rare (eg. Ishwara-Chandra & Saikia 1999), it is not unexpected that our sample is mostly composed by relatively nearby radio galaxies.

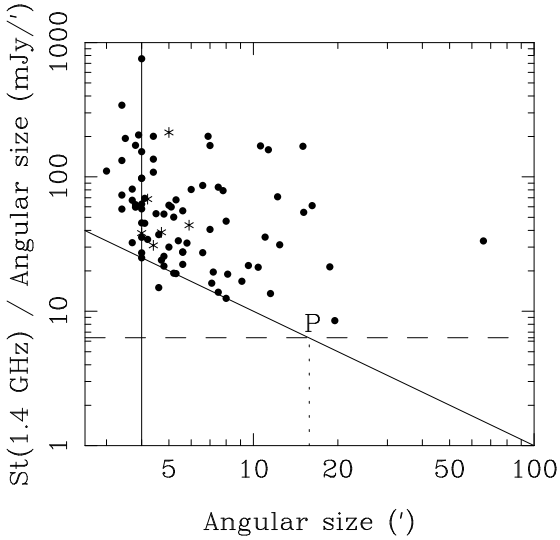


Fig. 3. Integrated flux density per length unit against the source angular length. The vertical and the oblique solid lines represent the sample limits in angular size ($\geq 4'$) and flux density ($S_t^{1.4} \geq 100$ mJy), respectively. The dashed horizontal line represents the sensitivity limit of the NVSS (see text). The vertical dotted line marks the angular size of $15.8'$, above which sources with a flux density greater than 100 mJy could be undetected in the NVSS (P point). Sources with uncertain redshift in Table 2 are represented with asterisks.

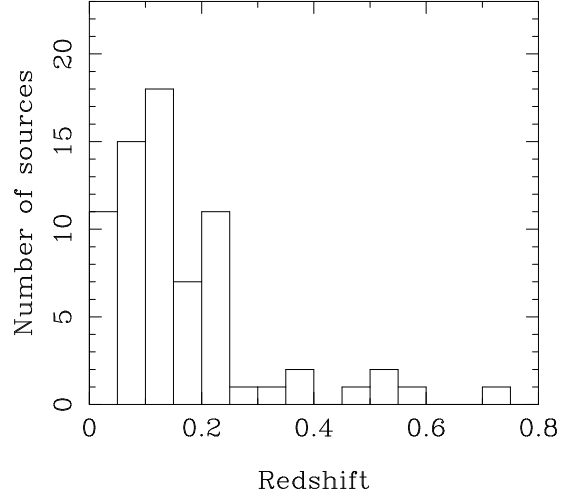


Fig. 4. Histogram of the distribution of redshifts in our sample. The redshift bin is 0.05.

The total radio power at 1.4 GHz as a function of the source redshift is represented in Fig. 5. The effect of the total flux density limitation ($S_t^{1.4} \geq 100$ mJy) is easily visible and shown by a solid line. This limitation masks any possible trend of the radio power distribution with the redshift, although we note the small number of nearby ($z \leq 0.1$) high power ($\log P_t^{1.4} \geq 25.5$) radio sources in the sample. Similarly, if we represent the source linear sizes against their redshifts (Fig. 6), we find a small number of giant radio galaxies with $z \leq 0.1$. We plot in Fig. 6 a dashed line which represents the locus of a 100 mJy $16'$ large radio source in this diagram (P point in Fig. 3), to give an idea of the sensitivity limit of the NVSS. We find that GRGs with $z \leq 0.04$ could be below the detection limit. However, the dashed line does not define a stringent limit since the real brightness distribution of radio sources is not rectangular and uniform as we have previously assumed. In consequence, much larger sources could be detected and, in fact, we find a low redshift source in our sample above that limit: J1632+825 (NGC 6251; dominated by a strong narrow jet).

The lack of small size sources at high redshift is entirely related to our selection limit of $4'$ in size (solid line; there are sources below the line, which correspond to sources smaller than $4'$ in Table 2). Moreover, we have a few giant radio galaxies at high redshift ($z \geq 0.5$). From previous studies (eg. Schoenmakers et al. 2000, Lara et al. 2000) it was derived that giant sources are characterized by large spectral ages. The existence of giant radio galaxies at high redshift would then imply that old radio sources are present at $z \geq 0.5$.

Another question raised after a first inspection of the sample is why we do not find radio sources with linear sizes below 200 Kpc. From Fig. 6 we find that intrinsically small sources should have redshifts below 0.03 to fit the size limit of $4'$. We have 6 sources below this redshift, but with angular sizes above $7'$. The absence of small nearby sources

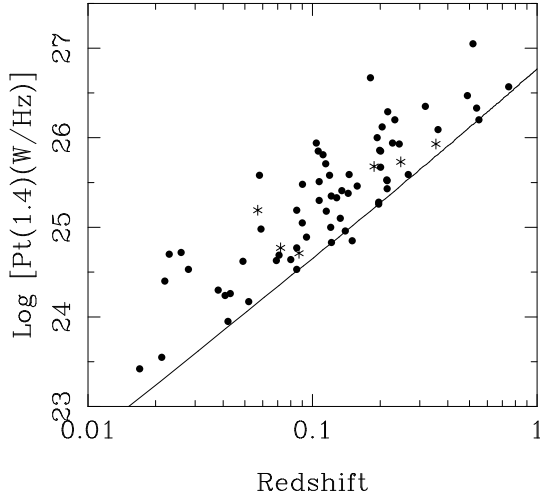


Fig. 5. Luminosities of the members of the sample plotted against their redshifts. The solid line represents the flux density limit imposed by our selection criteria ($S_t^{1.4} \geq 100$ mJy). Sources with uncertain redshift in Table 2 are represented with asterisks.

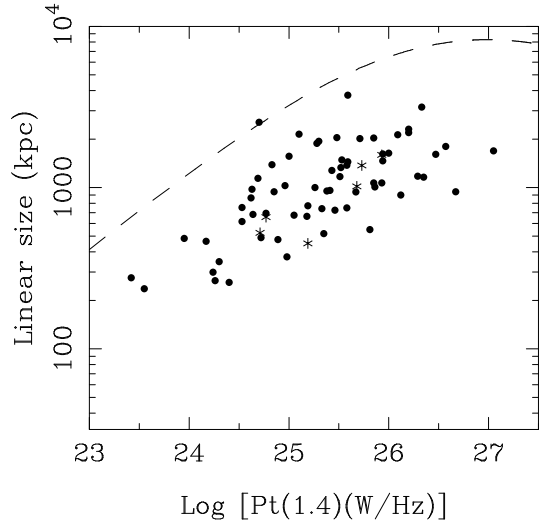


Fig. 7. Projected linear sizes of the members of the sample plotted against their luminosities. The dashed line represents the same sensitivity limit shown in Fig. 6. Sources with uncertain redshift in Table 2 are represented with asterisks.

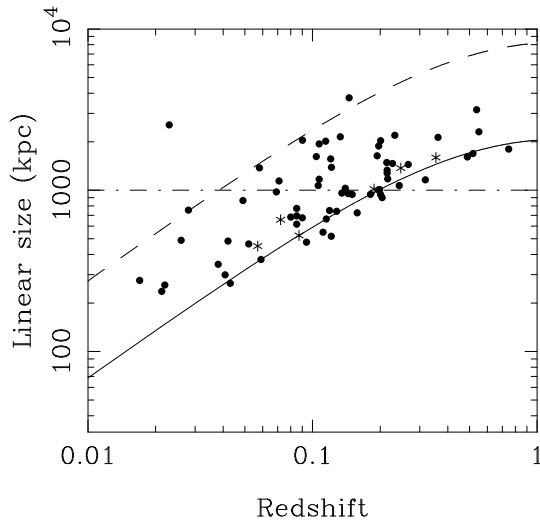


Fig. 6. Projected linear distance against redshift. The solid line indicates the limit imposed by our selection criteria (as in Fig. 3, there are some sources smaller than $4'$). The dashed line represents the sensitivity limit of the NVSS for a $16'$ extended 100 mJy source (see text). The horizontal dotted line marks the usual definition of giant radio galaxies. Sources with uncertain redshift in Table 2 are represented with asterisks.

must be related with the radio galaxy population and the small volume enclosed at low redshifts. There exist indeed sources smaller than 100 Kpc which fit our requirements, but must be rare (one example should be Cen A, if it were at declinations above $+60^\circ$).

In Fig. 7 we have plotted the source projected linear size versus the source total radio power at 1.4 GHz. The dotted line represents the “limit” due to sensitivity limitations of the NVSS, as in Fig. 6. We find a striking absence of intrinsically small high power radio galaxies. All sources

with sizes below 500 Kpc have $\log P_t(1.4)$ below 25.5. Since our criteria require that sources smaller than 500 Kpc be at $z \leq 0.1$, this is not a selection effect and must be a consequence of the statistically low number of sources with high radio power enclosed in the limited volume given by $z < 0.1$. Nearby sources have, in general, low power.

Finally, we plot in Fig. 8 a histogram of the core flux density at 4.9 GHz, up to 100 mJy. There are 5 sources with a core flux density above this value and therefore not represented in this plot. We note that our selection criteria do not impose restrictions on the core flux density and in fact, 51 out of 84 radio sources have weak cores, below 10 mJy. This is an expected result, since our sample selection criteria do not favor jets pointing toward the observer and, consequently, we do not expect relativistic Doppler boosting of intrinsically weak cores. However, the study of the parsec scale properties of the members of the sample by means of VLBI observations will require, in most cases, the use of the phase referencing technique in order to achieve enough sensitivity to properly map radio cores with a flux density below 10-20 mJy.

6. Conclusions

We have presented in this paper a new sample of 84 large angular size radio galaxies selected from the NVSS, with total flux density at 1.4 GHz ≥ 100 mJy and declination above $+60^\circ$. The selection has been made using high resolution and sensitive VLA observations at 1.4 and 4.9 GHz, which allowed us to properly map extended structures and to determine the radio core position. We measured new redshifts for 44 radio sources (Paper II).

We have discussed selection effects and limits. Within our selection criteria the final sample is homogeneous and can be used for statistical studies (Paper III).

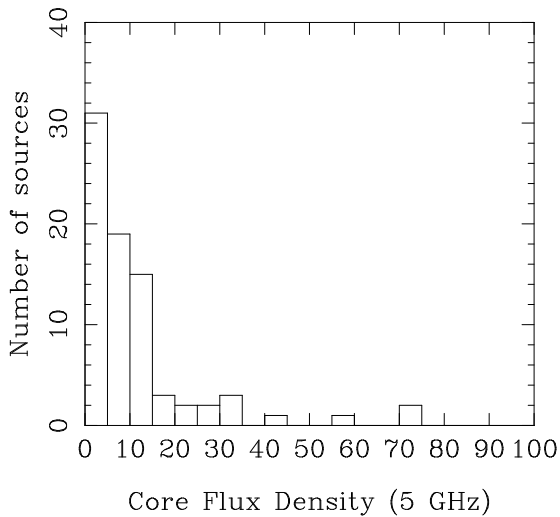


Fig. 8. Histogram of the core flux density of the sample sources at 4.9 GHz, up to 100 mJy. The bin size is 5 mJy.

37 radio sources in our sample have a linear size larger than 1 Mpc, of which 22 are new. Adding to these the sample of GRGs by Schoenmakers (1999) and the compilation of GRGs from literature data by Ishwara-Chandra & Saikia (1999), the number of known GRGs rises to 103, which allows a detailed study of the properties of this poorly known class of radio sources.

Acknowledgements. This research is supported in part by the Spanish DGICYT (PB97-1164). GG and LF acknowledge the Italian Ministry for University and Research (MURST) for financial support under grant Cofin98-02-32. The National Radio Astronomy Observatory is a facility of the National Science Foundation operated under cooperative agreement by Associated Universities, Inc. This research has made use of the NASA/IPAC Extragalactic Database (NED) which is operated by the Jet Propulsion Laboratory, California Institute of Technology, under contract with the National Aeronautics and Space Administration.

References

- van Breugel W. & Jägers W., 1982, *A&AS*, 49, 529
 Condon J.J., Cotton W.D., Greisen E.W., Yin Q.F., Perley R.A., Taylor G.B., Broderick J.J., 1998, *AJ*, 115, 1693
 Fanaroff B.L. & Riley J.M., 1974, *MNRAS*, 167, 31
 Fomalont E.B., Frey S., Paragi Z., Gurvits L.I., Scott W.K., Taylor A.R., Edwards P.G., Hirabayashi H., 2000, *ApJS*, 131, 95
 Giovannini G., Cotton W.D., Feretti L., Lara L., Venturi T., 1998, *ApJ*, 493, 632
 Ishwara-Chandra C.H. & Saikia D.J., 1999, *MNRAS*, 309, 100
 Jägers W.J., 1986, Ph. D. thesis, University of Leiden
 Kellermann K.I., Vermeulen R.C., Zensus J.A., Cohen M.H., 1998, *AJ*, 115, 1295
 Lara L., Márquez I., Cotton W.D., Feretti L., Giovannini G., Marcaide J.M., Venturi T., 1999, *A&A*, 348, 699
 Lara L., Márquez I., Cotton W.D., Feretti L., Giovannini G., Marcaide J.M., Venturi T., 1999, *NewAR*, 43, 643
 Lara L., Mack K.-H., Lacy M., Klein U., Cotton W.D., Feretti L., Giovannini G., Murgia M., 2000, *A&A*, 356, 63
 Leahy J.P., Bridle A.H., Strom R.G., 1998, *DRAGN Atlas*, <http://www.jb.man.ac.uk/atlas>
 Mack K.-H., 1996, Ph. D. thesis, University of Bonn
 Marcha M.J.M., Browne I.W.A., Impey C.D., Smith P.S., 1996, *MNRAS*, 281, 425
 Palma C., Bauer F.E., Cotton W.D., Bridle A.H., Majewski S.R., Sarazin C.L., *AJ*, 119, 2068
 Pearson T.J. & Readhead A.C.S., 1988, *ApJ*, 328, 114
 Pearson T.J., Blundell K.M., Riley J.M., Warner P.J., 1992, *MNRAS*, 259, L13
 Perley R.A., Bridle A.H., Willis A.G., 1984, *ApJS*, 54, 291
 Perley R.A. & Taylor G.B., 2000, *The VLA Calibrator Manual*, <http://www.aoc.nrao.edu/~taylor/calib.html>
 Polatidis A.G., Wilkinson P.N., Xu W., Readhead A.C.S., Pearson T.J., Taylor G.B., Vermeulen R.C., 1995, *ApJS*, 98, 1
 Reid A., Shone D.L., Akujor C.E., Browne I.W.A., Murphy D.W., Pedelty J., Rudnick L., Walsh D., 1995, *A&AS*, 110, 213
 Rengelink R.B., Tang Y., de Bruyn A.G., Miley G.K., Bremer M.N., Röttgering H.J.A., Bremer M.R.A., 1997, *A&AS*, 124, 259
 Riley J.M., Warner P.J., Rawlings S., Saunders R., Pooley G.G., Eales S.A., 1989, *MNRAS*, 236, L13
 Saripalli L., Patnaik A.R., Porcas R.W., Graham D.A., 1997, *A&A*, 328, 78
 Schoenmakers A.P., Mack K.-H., Lara L., Röttgering H.J.A., de Bruyn A.G., van der Laan H., Giovannini G., 1998, *A&A*, 336, 455
 Schoenmakers A.P., 1999, Ph. D. thesis, University of Utrecht
 Schoenmakers A.P., Mack K.-H., de Bruyn A.G., Röttgering H.J.A., Klein U., van der Laan H., *A&AS*, 146, 293
 Stickle M., Kühr H., Fried J.W., 1993, *A&AS*, 97, 483
 Taylor G.B., Vermeulen R.C., Pearson T.J., Readhead A.C.S., Henstock D.R., Browne I.W.A., Wilkinson P.N., 1994, *ApJS*, 95, 345
 Urry C.M. & Padovani P., 1995, *PASP*, 107, 803
 de Vries W.H., Barthel P.D., O’Dea C.P., 1997, *A&A*, 321, 105

This figure "fig2_1.gif" is available in "gif" format from:

<http://arxiv.org/ps/astro-ph/0102034v1>

This figure "fig2_2.gif" is available in "gif" format from:

<http://arxiv.org/ps/astro-ph/0102034v1>

This figure "fig2_3.gif" is available in "gif" format from:

<http://arxiv.org/ps/astro-ph/0102034v1>

This figure "fig2_4.gif" is available in "gif" format from:

<http://arxiv.org/ps/astro-ph/0102034v1>

This figure "fig2_5.gif" is available in "gif" format from:

<http://arxiv.org/ps/astro-ph/0102034v1>

This figure "fig2_6.gif" is available in "gif" format from:

<http://arxiv.org/ps/astro-ph/0102034v1>

This figure "fig2_7.gif" is available in "gif" format from:

<http://arxiv.org/ps/astro-ph/0102034v1>

This figure "fig2_8.gif" is available in "gif" format from:

<http://arxiv.org/ps/astro-ph/0102034v1>

This figure "fig2_9.gif" is available in "gif" format from:

<http://arxiv.org/ps/astro-ph/0102034v1>

This figure "fig2_10.gif" is available in "gif" format from:

<http://arxiv.org/ps/astro-ph/0102034v1>

This figure "fig2_11.gif" is available in "gif" format from:

<http://arxiv.org/ps/astro-ph/0102034v1>

This figure "fig2_12.gif" is available in "gif" format from:

<http://arxiv.org/ps/astro-ph/0102034v1>

This figure "fig2_13.gif" is available in "gif" format from:

<http://arxiv.org/ps/astro-ph/0102034v1>

This figure "fig2_14.gif" is available in "gif" format from:

<http://arxiv.org/ps/astro-ph/0102034v1>

This figure "fig2_15.gif" is available in "gif" format from:

<http://arxiv.org/ps/astro-ph/0102034v1>

This figure "fig2_16.gif" is available in "gif" format from:

<http://arxiv.org/ps/astro-ph/0102034v1>

This figure "fig2_17.gif" is available in "gif" format from:

<http://arxiv.org/ps/astro-ph/0102034v1>

This figure "fig2_18.gif" is available in "gif" format from:

<http://arxiv.org/ps/astro-ph/0102034v1>

This figure "fig2_19.gif" is available in "gif" format from:

<http://arxiv.org/ps/astro-ph/0102034v1>

This figure "fig2_20.gif" is available in "gif" format from:

<http://arxiv.org/ps/astro-ph/0102034v1>

This figure "fig2_21.gif" is available in "gif" format from:

<http://arxiv.org/ps/astro-ph/0102034v1>

This figure "fig2_22.gif" is available in "gif" format from:

<http://arxiv.org/ps/astro-ph/0102034v1>

This figure "fig2_23.gif" is available in "gif" format from:

<http://arxiv.org/ps/astro-ph/0102034v1>

This figure "fig2_24.gif" is available in "gif" format from:

<http://arxiv.org/ps/astro-ph/0102034v1>

This figure "fig2_25.gif" is available in "gif" format from:

<http://arxiv.org/ps/astro-ph/0102034v1>

This figure "fig2_26.gif" is available in "gif" format from:

<http://arxiv.org/ps/astro-ph/0102034v1>

This figure "fig2_27.gif" is available in "gif" format from:

<http://arxiv.org/ps/astro-ph/0102034v1>

This figure "fig2_28.gif" is available in "gif" format from:

<http://arxiv.org/ps/astro-ph/0102034v1>